Search for Short Transient Neutrino Emission with IceCube-DeepCore

IceCube Collaboration: M. G. Aartsen[1], K. Abraham[2], M. Ackermann[3], J. Adams[4], J. A. Aguilar[5], M. Ahlers[6], M. Ahrens[7], D. Altmann[8], T. Anderson[9], I. Ansseau[5], M. Archinger[10], C. Arguelles[6], T. C. Arlen[9], J. Auffenberg[11], X. Bai[12], S. W. Barwick[13], V. Baum[10], R. Bay[14], J. J. Beatty[15,16], J. Becker Tjus[17], K.-H. Becker[18], E. Beiser[6], S. BenZvi[6], P. Berghaus[3], D. Berley[19], E. Bernardini[3], A. Bernhard[2], D. Z. Besson[20], G. Binder[21,14], D. Bindig[18], M. Bissok[11], E. Blaufuss[19], J. Blumenthal[11], D. J. Boersma[22], C. Bohm[7], M. Börner[23], F. Bos[17], D. Bose[24], S. Böser[10], O. Botner[22], J. Braun[6], L. Brayeur[25], H.-P. Bretz[3], N. Buzinsky[26], J. Casey[27], M. Casier[25], E. Cheung[19], D. Chirkin[6], A. Christov[28], K. Clark[29], L. Classen[8], S. Coenders[2], D. F. Cowen[9,30], A. H. Cruz Silva[3], J. Daughhetee[27], J. C. Davis[15], M. Day[6], J. P. A. M. de André[31], C. De Clercq[25], E. del Pino Rosendo[10], H. Dembinski[32], S. De Ridder[33], P. Desiati[6], K. D. de Vries[25], G. de Wasseige[25], M. de With[34], T. DeYoung[31], J. C. Díaz-Vélez[6], V. di Lorenzo[10], J. P. Dumm[7], M. Dunkman[9], R. Eagan[9], B. Eberhardt[10], T. Ehrhardt[10], B. Eichmann[17], S. Euler[22], P. A. Evenson[32], O. Fadiran[6], S. Fahey[6], A. R. Fazely[35], A. Fedynitch[17], J. Feintzeig[6], J. Felde[19], K. Filimonov[14], C. Finley[7], T. Fischer-Wasels[18], S. Flis[7], C.-C. Fösig[10], T. Fuchs[23], T. K. Gaisser[32], R. Gaior[36], J. Gallagher[37], L. Gerhardt[21,14], K. Ghorbani[6], D. Gier[11], L. Gladstone[6], M. Glagla[11], T. Glüsenkamp[3], A. Goldschmidt[21], G. Golup[25], J. G. Gonzalez[32], D. Góra[3], D. Grant[26], J. C. Groh[9], A. Groß[2], C. Ha[21,14], C. Haack[11], A. Haj Ismail[33], A. Hallgren[22], F. Halzen[6], B. Hansmann[11], K. Hanson[6], D. Hebecker[34], D. Heereman[5], K. Helbing[18], R. Hellauer[19], D. Hellwig[11], S. Hickford[18], J. Hignight[31], G. C. Hill[1], K. D. Hoffman[19], R. Hoffmann[18], K. Holzapfel[2], A. Homeier[38], K. Hoshina[6,49], F. Huang[9], M. Huber[2], W. Huelsnitz[19], P. O. Hulth[7], K. Hultqvist[7], S. In[24], A. Ishihara[36], E. Jacobi[3], G. S. Japaridze[39], K. Jero[6], M. Jurkovic[2], B. Kaminsky[3], A. Kappes[8], T. Karg[3], A. Karle[6], M. Kauer[6,40], A. Keivani[9],

J. L. Kelley[6], J. Kemp[11], A. Kheirandish[6], J. Kiryluk[41], J. Kläs[18], S. R. Klein[21,14], G. Kohnen[42], R. Koirala[32], H. Kolanoski[34], R. Konietz[11], A. Koob[11], L. Köpke[10], C. Kopper[26], S. Kopper[18], D. J. Koskinen[43], M. Kowalski[34,3], K. Krings[2], G. Kroll[10], M. Kroll[17], J. Kunnen[25], N. Kurahashi[44], T. Kuwabara[36], M. Labare[33], J. L. Lanfranchi[9], M. J. Larson[43], M. Lesiak-Bzdak[41], M. Leuermann[11], J. Leuner[11], J. Lünemann[10], J. Madsen[45], G. Maggi[25], K. B. M. Mahn[31], R. Maruyama[40], K. Mase[36], H. S. Matis[21], R. Maunu[19], F. McNally[6], K. Meagher[5], M. Medici[43], A. Meli[33], T. Menne[23], G. Merino[6], T. Meures[5], S. Miarecki[21,14], E. Middell[3], E. Middlemas[6], J. Miller[25], L. Mohrmann[3], T. Montaruli[28], R. Morse[6], R. Nahnhauer[3], U. Naumann[18], H. Niederhausen[41], S. C. Nowicki[26], D. R. Nygren[21], A. Obertacke[18], A. Olivas[19], A. Omairat[18], A. O'Murchadha[5], T. Palczewski[46], H. Pandya[32], L. Paul[11], J. A. Pepper[46], C. Pérez de los Heros[22], C. Pfendner[15], D. Pieloth[23], E. Pinat[5], J. Posselt[18], P. B. Price[14], G. T. Przybylski[21], J. Pütz[11], M. Quinnan[9], C. Raab[5], L. Rädel[11], M. Rameez[28], K. Rawlins[47], R. Reimann[11], M. Relich[36], E. Resconi[2], W. Rhode[23], M. Richman[44], S. Richter[6], B. Riedel[26], S. Robertson[1], M. Rongen[11], C. Rott[24], T. Ruhe[23], D. Ryckbosch[33], S. M. Saba[17], L. Sabbatini[6], H.-G. Sander[10], A. Sandrock[23], J. Sandroos[10], S. Sarkar[43,48], K. Schatto[10], F. Scheriau[23], M. Schimp[11], T. Schmidt[19], M. Schmitz[23], S. Schoenen[11], S. Schöneberg[17], A. Schönwald[3], L. Schulte[38], D. Seckel[32], S. Seunarine[45], R. Shanidze[3], M. W. E. Smith[9], D. Soldin[18], M. Song[19], G. M. Spiczak[45], C. Spiering[3], M. Stahlberg[11], M. Stamatikos[15,50], T. Stanev[32], N. A. Stanisha[9], A. Stasik[3], T. Stezelberger[21], R. G. Stokstad[21], A. Stößl[3], E. A. Strahler[25], R. Ström[22], N. L. Strotjohann[3], G. W. Sullivan[19], M. Sutherland[15], H. Taavola[22], I. Taboada[27], S. Ter-Antonyan[35], A. Terliuk[3], G. Tešić[9], S. Tilav[32], P. A. Toale[46], M. N. Tobin[6], D. Tosi[6], M. Tselengidou[8], A. Turcati[2], E. Unger[22], M. Usner[3], S. Vallecorsa[28], J. Vandenbroucke[6], N. van Eijndhoven[25], S. Vanheule[33], J. van Santen[6], J. Veenkamp[2], M. Vehring[11], M. Voge[38], M. Vraeghe[33], C. Walck[7], A. Wallace[1], M. Wallraff[11], N. Wandkowsky[6],

Ch. Weaver[26], C. Wendt[6], S. Westerhoff[6], B. J. Whelan[1], N. Whitehorn[6], C. Wichary[11], K. Wiebe[10], C. H. Wiebusch[11], L. Wille[6], D. R. Williams[46], H. Wissing[19], M. Wolf[7], T. R. Wood[26], K. Woschnagg[14], D. L. Xu[46], X. W. Xu[35], Y. Xu[41], J. P. Yanez[3], G. Yodh[13], S. Yoshida[36], and M. Zoll[7]

[1]Department of Physics, University of Adelaide, Adelaide, 5005, Australia

[2]Technische Universität München, D-85748 Garching, Germany

[3]DESY, D-15735 Zeuthen, Germany

[4]Dept. of Physics and Astronomy, University of Canterbury, Private Bag 4800, Christchurch, New Zealand

[5]Université Libre de Bruxelles, Science Faculty CP230, B-1050 Brussels, Belgium

[6]Dept. of Physics and Wisconsin IceCube Particle Astrophysics Center, University of Wisconsin, Madison, WI 53706, USA

[7]Oskar Klein Centre and Dept. of Physics, Stockholm University, SE-10691 Stockholm, Sweden

[8]Erlangen Centre for Astroparticle Physics, Friedrich-Alexander-Universität Erlangen-Nürnberg, D-91058 Erlangen, Germany

[9]Dept. of Physics, Pennsylvania State University, University Park, PA 16802, USA

[10]Institute of Physics, University of Mainz, Staudinger Weg 7, D-55099 Mainz, Germany

[11]III. Physikalisches Institut, RWTH Aachen University, D-52056 Aachen, Germany

[12]Physics Department, South Dakota School of Mines and Technology, Rapid City, SD 57701, USA

[13]Dept. of Physics and Astronomy, University of California, Irvine, CA 92697, USA

[14]Dept. of Physics, University of California, Berkeley, CA 94720, USA

[15]Dept. of Physics and Center for Cosmology and Astro-Particle Physics, Ohio State University, Columbus, OH 43210, USA

[16]Dept. of Astronomy, Ohio State University, Columbus, OH 43210, USA

[17]Fakultät für Physik & Astronomie, Ruhr-Universität Bochum, D-44780 Bochum, Germany

[18]Dept. of Physics, University of Wuppertal, D-42119 Wuppertal, Germany

[19]Dept. of Physics, University of Maryland, College Park, MD 20742, USA

[20]Dept. of Physics and Astronomy, University of Kansas, Lawrence, KS 66045, USA

[21]Lawrence Berkeley National Laboratory, Berkeley, CA 94720, USA

[22]Dept. of Physics and Astronomy, Uppsala University, Box 516, S-75120 Uppsala, Sweden

[23]Dept. of Physics, TU Dortmund University, D-44221 Dortmund, Germany

[24]Dept. of Physics, Sungkyunkwan University, Suwon 440-746, Korea

[25]Vrije Universiteit Brussel, Dienst ELEM, B-1050 Brussels, Belgium

[26]Dept. of Physics, University of Alberta, Edmonton, Alberta, Canada T6G 2E1

[27]School of Physics and Center for Relativistic Astrophysics, Georgia Institute of Technology, Atlanta, GA 30332, USA

[28]Département de physique nucléaire et corpusculaire, Université de Genève, CH-1211 Genève, Switzerland

[29]Dept. of Physics, University of Toronto, Toronto, Ontario, Canada, M5S 1A7

[30]Dept. of Astronomy and Astrophysics, Pennsylvania State University, University Park, PA 16802, USA

[31]Dept. of Physics and Astronomy, Michigan State University, East Lansing, MI 48824, USA

[32]Bartol Research Institute and Dept. of Physics and Astronomy, University of Delaware, Newark, DE 19716, USA

[33]Dept. of Physics and Astronomy, University of Gent, B-9000 Gent, Belgium

[34]Institut für Physik, Humboldt-Universität zu Berlin, D-12489 Berlin, Germany

[35]Dept. of Physics, Southern University, Baton Rouge, LA 70813, USA

[36]Dept. of Physics, Chiba University, Chiba 263-8522, Japan

[37]Dept. of Astronomy, University of Wisconsin, Madison, WI 53706, USA

[38]Physikalisches Institut, Universität Bonn, Nussallee 12, D-53115 Bonn, Germany

[39]CTSPS, Clark-Atlanta University, Atlanta, GA 30314, USA

[40]Dept. of Physics, Yale University, New Haven, CT 06520, USA

57 Received _____; accepted _____

[41]Dept. of Physics and Astronomy, Stony Brook University, Stony Brook, NY 11794-3800, USA

[42]Université de Mons, 7000 Mons, Belgium

[43]Niels Bohr Institute, University of Copenhagen, DK-2100 Copenhagen, Denmark

[44]Dept. of Physics, Drexel University, 3141 Chestnut Street, Philadelphia, PA 19104, USA

[45]Dept. of Physics, University of Wisconsin, River Falls, WI 54022, USA

[46]Dept. of Physics and Astronomy, University of Alabama, Tuscaloosa, AL 35487, USA

[47]Dept. of Physics and Astronomy, University of Alaska Anchorage, 3211 Providence Dr., Anchorage, AK 99508, USA

[48]Dept. of Physics, University of Oxford, 1 Keble Road, Oxford OX1 3NP, UK

[49]Earthquake Research Institute, University of Tokyo, Bunkyo, Tokyo 113-0032, Japan

[50]NASA Goddard Space Flight Center, Greenbelt, MD 20771, USA

58 ## ABSTRACT

59 We present the results of a search for astrophysical sources of brief transient neutrino emission using IceCube and DeepCore data acquired between May 15th 2012 and April 30th 2013. While the search methods employed in this analysis are similar to those used in previous IceCube point source searches, the data set being examined consists of a sample of predominantly sub-TeV muon neutrinos from the Northern Sky (-5° $< \delta <$ 90°) obtained through a novel event selection method. This search represents a first attempt by IceCube to identify astrophysical neutrino sources in this relatively unexplored energy range. The reconstructed direction and time of arrival of neutrino events is used to search for any significant self-correlation in the dataset. The data revealed no significant source of transient neutrino emission. This result has been used to construct limits on generic soft-spectra transients as well as a specific model of neutrino emission from soft jets in core-collapse supernovae.

60 *Subject headings:* neutrino astronomy, neutrinos, GRB, supernova, astroparticle
61 physics

1. Introduction

The nascent field of high-energy neutrino astronomy opens the possibility of answering several open questions in astrophysics due in large part to the neutrino's ability to escape the densest regions of astrophysical environments. Specifically, the detection of transient astrophysical neutrino sources will help shed light on the acceleration mechanisms at work in some of the most energetic phenomena in the Universe such as gamma-ray bursts, supernovae, and active galactic nuclei. Previous attempts to detect such sources with the IceCube Neutrino Observatory (IceCube Collaboration et al. 2006) are most sensitive to neutrino fluxes above 1 TeV with poor sensitivity below 100 GeV. Searches for astrophysical sources at lower energies (1–100 GeV) have been performed by Super-Kamiokande (Thrane et al. 2009), however the detector's 50 kton instrumented volume limits its sensitivity to astrophysical neutrino fluxes. A newly developed 30–300 GeV muon neutrino sample collected by IceCube and its low energy extension DeepCore (Abbasi et al. 2012) seeks to enhance IceCube's sensitivity in this under-explored energy range. In this paper we will present the results of a search for transient neutrino emission in this GeV-scale neutrino sample.

The detection of astrophysical neutrino sources is a primary design goal of the IceCube Neutrino Observatory (IceCube Collaboration et al. 2006). Located at the geographic South Pole, IceCube utilizes the clear Antarctic glacial ice ice cap as a detection medium for the Cherenkov light produced by secondary products of neutrino interactions. The detector consists of 5,160 Digital Optical Modules (DOMs) distributed among 86 cables to form a 1 km^3 instrumented volume. These DOMs house photomultiplier tubes (PMTs), to detect Cherenkov photons, as well as digitizing electronics for initial processing of the PMT data. A centrally located region of denser instrumentation featuring DOMs with more sensitive PMTs comprises the DeepCore sub-array. This extension to the IceCube array enhances

the detector's response to lower energy neutrino events.

Typical searches for astrophysical sources with IceCube make use of a sample primarily comprised of an irreducible background of high-energy atmospheric muon neutrinos ($E_\nu \gtrsim 1$ TeV) to look for both steady (Aartsen et al. 2014b) and transient sources (Aartsen et al. 2015). As of yet, these searches have not found any significant self-correlations within the data sample nor correlations between the neutrino data and known astrophysical objects of interest. So far, these analyses have largely eschewed low energy neutrino events collected by DeepCore for two reasons. First, the poorer angular resolution of these events renders them less suitable for pointing analyses. Second, the soft spectrum of the atmospheric neutrino flux results in higher rate of background neutrino events. However, these issues of increased background can be somewhat mitigated by searching solely for transient sources. Therefore, applying previously developed search techniques (as described in Braun et al. (2010)) to a sample of low energy (30 GeV $\leq E_\nu <$ 300 GeV) muon neutrino events from DeepCore can enhance IceCube's sensitivity to short transient neutrino sources with softer spectra.

Due to the large atmospheric neutrino background in this energy range, searches using a data set composed of these low energy events will only be sensitive to emission timescales on the order of one day or shorter. Active galactic nuclei (AGN) undergoing flaring events are one potential source for emission on this timescale. Protons may be accelerated in relativistic jets, powered by accretion onto the AGN, resulting in the production of pions (and subsequently neutrinos) in shocks due to proton-photon interactions and proton self-collisions (Becker & Biermann 2009). Brief periods of enhanced accretion would then result in a commensurate increase in the neutrino flux from the AGN, which may be detectable using time-dependent search methods. Sub-photospheric neutrino emission from gamma-ray bursts (GRBs) represents another possible source for this search. A model

for photospheric gamma-ray emission in GRBs by Murase et al. (2013) suggests that a substantial flux of 100 GeV-scale neutrinos may be produced during the initial stages of relativistic outflow in the GRB. Decoupling of protons and neutrons during the initial formation of the relativistic jet causes hadronuclear collisions resulting in the production of pions and the production of neutrinos via pion decay. The predicted energy for the neutrinos produced in these sub-photospheric collisions is on the order of 100 GeV, and therefore this GRB neutrino flux may only be visible to IceCube searches with the inclusion of sub-TeV neutrino events.

Perhaps the most promising potential source for this study is a special class of core-collapse supernova referred to as a choked GRB [citation needed]. The standard GRB model assumes that relativistic jets are generated during the accretion of material onto the compact object formed during core-collapse (Rees & Meszaros 1992). Fermi-acceleration of charged particles occurs within the internal shocks of these jets leading to gamma ray emission once the jets breach the surrounding stellar envelope. There is an observed correlation between long duration GRBs and core-collapse supernovae (SNe) ((Woosley & Bloom 2006), (Modjaz 2011)). The observed fraction of SNe resulting in the occurrence of a GRB is quite low, however, it may be that a larger fraction of core-collapse SNe still manage to produce mildly relativistic jets. Due to insufficient energy, these jets fail to break through the stellar envelope and any gamma ray emission is effectively 'choked' off. If protons are accelerated in these jets, then neutrino production will occur in the shocks of the jet irrespective of whether or not the jet successfully escapes. A model of this neutrino emission proposed by Razzaque et al. (2004) and extended upon by Ando & Beacom (2005), hereafter referred to as the RMW/AB model, suggests that these neutrinos may be detectable by IceCube-DeepCore for nearby supernovae (Taboada 2010).

We present the results of a search for transient neutrino emission with a set of

low-energy neutrino event data collected from May 15th, 2012 to April 30th, 2013. The data selection methods used to acquire this unique event sample will be detailed in Sec. 2. Analysis methods and search techniques are discussed in Sec. 3. Finally, the results of the search are given in Sec. 4 in addition to how these results may be interpreted within the context of generic neutrino flares as well as choked GRBs under the RMW/AB model.

2. Event Selection

The data acquisition process begins with the fulfillment of one of three trigger conditions that prompt readout of the detector data. Each of these triggers requires some number of DOMs to exhibit hard local coincidence within a defined time window. To satisfy the hard local coincidence (HLC) condition, two or more neighboring (or next-neighboring) DOMs on the same string must register photon hits within a ± 1 μs window. The trigger for the lowest energy events requires three HLC DOM hits within a time window of 2.5 μs among the DeepCore string DOMs (or in DOMs on IceCube strings neighboring DeepCore); it is often referred to as simple majority trigger 3 or SMT3. The two other triggers that serve as input for this event selection operate over the entire detector with one requiring eight HLC DOM hits in a 5 μs window (SMT8) and the other requiring four HLC DOM hits within a cylinder of height of 75m and a radius of 175m in a 1 μs window (Cylinder Trigger).

Events satisfying these trigger conditions are then given to the DeepCore data filter. This filter seeks to eliminate cosmic ray muons by using the outer regions of the detector as an active veto to tag down-going events originating outside the detector. Specifically, the filter examines timing and position information of DOM hits inside the DeepCore fiducial volume to create a center of gravity (CoG) or vertex. For each DOM hit in the veto region, the speed of a hypothetical particle connecting that veto region hit to the CoG inside the

fiducial volume is calculated. Veto regions hits whose speed lies within a range consistent with that of the speed of light are causally related and are therefore likely the product of background cosmic ray muons. Events having more than one correlated veto region hit are removed by the filter. A more complete description of this filter can be found in Abbasi et al. (2012).

During the observation period of this search, the DeepCore filter consists of two separate branches characterized by differing definitions of detection and veto volumes as opposed to the single definition given in Abbasi et al. (2012). Another key difference of the filter with respect to the definition provided in Abbasi et al. (2012) is that it now makes use of some isolated DOM hit information instead of only using HLC hits. Events satisfying the SMT3 trigger feed the standard DeepCore filter branch whose fiducial and veto region definitions are roughly equivalent to those described in Abbasi et al. (2012). The SMT8 and Cylinder Trigger events, in addition to SMT3 events that fail the standard filter branch, feed into the other branch of the filter which makes use of a more relaxed veto region. While the standard filter branch makes use of three surrounding layers of IceCube strings as a veto, this relaxed branch only uses two layers of IceCube strings for vetoing so that a larger detection volume may be used. The output of both branches of this filter are used in this search with the standard three-layer veto focusing on low-energy events and the two-layer veto branch retaining higher energy events. These branches are referred to as the low-energy stream (LES) and high-energy stream (HES), and they have an exclusive event rate of 17.25 Hz and 23.3 Hz respectively.

2.1. Veto Cuts and Event Reconstruction

Events belonging to both the LES and HES are subjected to several cuts that make use of veto region hit information, event topology, and event reconstructions to reduce the

volume of cosmic ray background events as well as eliminate events that are the result of PMT dark noise-induced triggering. The first of these cuts requires at least two DeepCore DOM hits within a tight 250 ns window to remove SMT3 events that are the result of spurious hits. An algorithm designed to search for track-like events is then used to eliminate noise-induced events that show little evidence of correlation in DOM hits. Additionally, a minimum on the number of DOMs registering light during the event (10) is imposed to throw out events with too little information for proper reconstruction. The DeepCore filter algorithm is also reapplied several times using looser DOM hit cleanings to allow more isolated DOM hits in the veto region to contribute to the vertex calculations. Finally, the number of DOM hits that occur prior to the first hit inside the DeepCore detection volume is used as a cut parameter to eliminate less obvious cosmic ray muons.

The event reconstruction process begins with the application of a simple linear fit described in Aartsen et al. (2014a) to determine the position of a muon track that describes the observed DOM hit pattern. This linear reconstruction is then used as a seed for a likelihood-based reconstruction which uses a single-photoelectron (SPE) hypothesis to describe the probability of DOMs receiving light from the track at a given time due to scattering in the ice (this algorithm is described in detail in Ahrens et al. (2004)). Six iterations of the SPE likelihood reconstruction are performed to obtain a best-fit track for the event. Any event whose reconstructed direction from either the linear or SPE likelihood fit is more than 5° above the horizon is removed from the sample. We also require that the angular separation between these two reconstructions is less than 30° for events in the HES sample.

The occurrence of spurious DOM hits in the central detector prior to the arrival of cosmic ray muons allows many background events to elude detection through the standard veto technique. To isolate these events, a separate SPE likelihood reconstruction is

performed without using any information from the first two DOM hits in the event. Just as before, events whose reconstructed direction lies more than 5° above the horizon are removed. Events in the LES portion of the sample are disproportionately affected by noise hits due to both the lower light yield of these events as well as the higher noise rate of the sensitive DeepCore DOMs. Therefore an additional SPE likelihood reconstruction is performed for LES events that attempts to mitigate noise contribution to the likelihood by requiring isolated DOM hits to be more strongly correlated to hits satisfying the HLC condition. Once again, if the best-fit direction from this additional reconstruction on LES events is 5° above the horizon, the event is removed.

The final event reconstruction makes use of the previously mentioned six iteration SPE likelihood fit as its seed. This reconstruction differs from the seed in two important ways. First, it makes use of a multi-photoelectron (MPE) likelihood instead of the simpler SPE algorithm used previously (see Ahrens et al. (2004) for more information on the MPE likelihood). Second, a parameterization of Monte Carlo simulation of photon transport is used in place of an analytic approximation to model the timing distribution for the arrival of Cherenkov photons to the DOM PMTs (Whitehorn et al. 2013). This reconstruction is identical to that used in a multi-year point source search with IceCube (Aartsen et al. 2014b) and the results of this fit are used for analysis of the final data. In order to estimated the angular uncertainty of the reconstruction, the likelihood space about the reconstructed direction is fit with a paraboloid via the method described in Neunhöffer (2006). The angular uncertainty derived from the paraboloid method serves as event quality parameter, and only events having an estimated angular error σ_i less than 45° are kept.

2.2. Boosted Decision Tree

After the application of the described veto and reconstruction cuts, the ability to separate muon background from potential neutrino signal events via simple cuts is drastically reduced. We therefore make use of a boosted decision tree (BDT) in order to isolate a final sample with acceptable neutrino purity, i.e. $< 10\%$ of events are the result of background cosmic ray muons. At this level of event selection, the large majority of experimental data still consists of background cosmic ray muons allowing the actual data to serve as a background training sample for the BDT. Simulated signal neutrino events belonging to the LES or HES branches exhibit significant differences in distribution of input BDT parameters necessitating the construction of two separate BDTs.

The event parameters used for the LES tree include the location of the reconstructed event vertex, the number of 'direct' DOM hits featuring a photon travel time residual between -25 and 150 ns with respect to the reconstructed muon track, the reduced log-likelihood of the MPE reconstruction, the average distance between DOM hits and the reconstructed track weighted by DOM photo-multiplier tube (PMT) charge, and the highest clustering of veto region PMT charge found by brute force reconstruction methods. The HES BDT makes use of the direct hits parameter, reduced log-likelihood of the MPE reconstruction, average charge-weighted DOM distance to track, and also the best fit track length using information from direct DOM hits. A simulated signal neutrino event sample weighted to a $E^{-2.5}$ (LES) or E^{-2} (HES) spectrum is used for signal training.

Events are then fed to the trained BDT which assigns the event a score which indicates the degree to which the event resembles signal or background. A cut on event BDT score is then imposed where the value of the BDT cut is chosen to obtain a neutrino purity of approximately 90%. The final event sample after the application of the BDT cuts consists of 22,040 events over a livetime of $\sim$330 days corresponding to a data rate of about 0.77

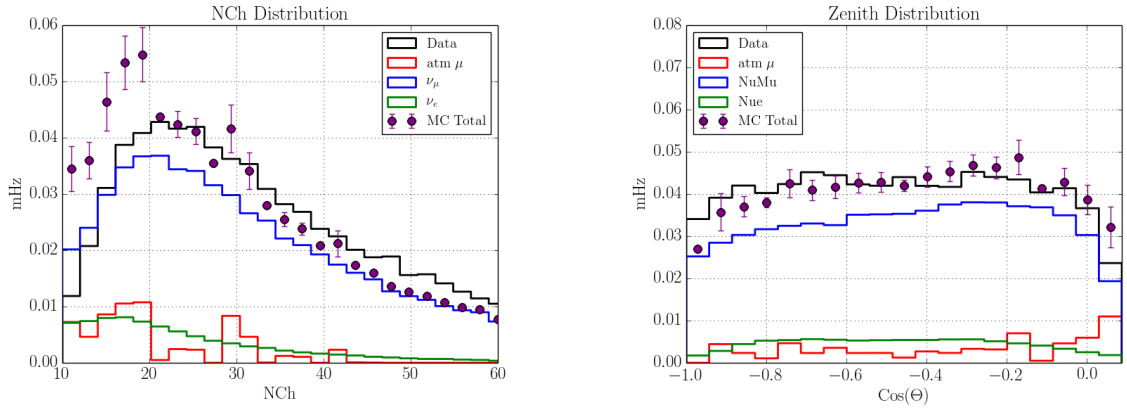

Fig. 1.— Final event rate distributions for the number of DOMs registering hits during the event (left) and the cosine of the reconstructed event zenith in detector coordinates (right).

mHz. As Figure 1 indicates, the final sample is mostly composed of atmospheric neutrinos with an estimated cosmic ray muon contamination of approximately 0.08 mHz. There is some disagreement between the predictions from simulation and the actual data (primarily the rate of events featuring a low number of DOM hits), and much of this discrepancy stems from limited statistics for cosmic ray muon simulation. This is not greatly concerning however, as we are able to measure the background directly from the final data set itself.

The neutrino effective area for this event selection is shown in Figure 2. While standard IceCube analyses clearly have superior sensitivity at higher energies, this event selection does show increased acceptance for events below about 100 GeV in primary neutrino energy. The angular resolution for events at the analysis level is plotted as a function of energy in Figure 2 as well. Lower neutrino energies result in muon tracks that are both shorter and dimmer which leads to difficulty in resolving the direction of the neutrino primary. The kinematic angle between the neutrino primary and muon secondary also contributes to angular error. The median kinematic muon-neutrino angle after event selection ranges from $\sim 3^\circ$ at 50 GeV to $\sim 1^\circ$ at 300 GeV. As the figure shows, the efficacy of the reconstruction method used in this analysis begins to deteriorate rapidly below 30 GeV due to insufficient

information (i.e. lack of DOM hits). Although the pointing ability of these low-energy neutrino events is limited, they are still able to contribute to the search through temporal correlation with other events in the sample.

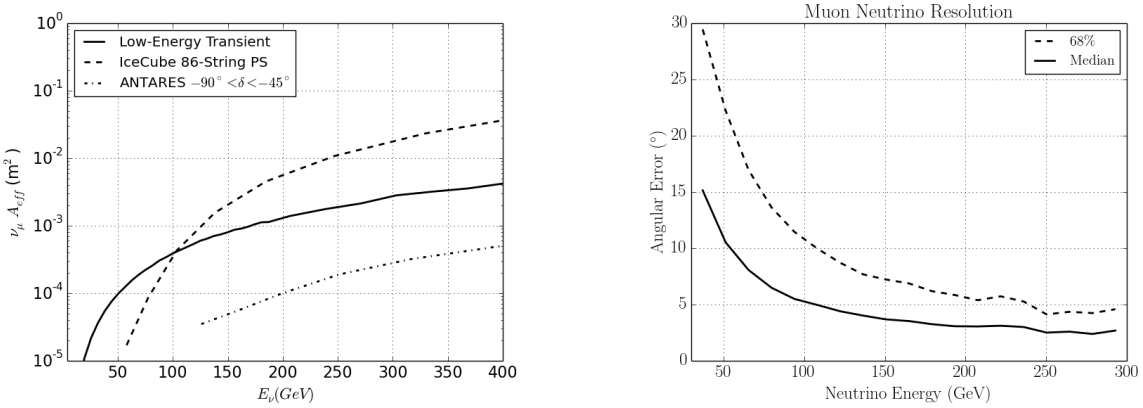

Fig. 2.— The muon neutrino effective area as a function of neutrino energy is plotted above (left) for the presented search. The effective areas for both the 4 year IceCube point source search (Aartsen et al. 2014b) and the 4 year ANTARES point source search (Adrián-Martínez et al. 2012) are plotted as well for comparison. Angular resolution as a function of energy after event selection is shown in the right plot.

3. Analysis Method

The search methods employed in the analysis of this data are nearly identical to those used in previous time-dependent IceCube analyses (see Braun et al. (2008) and Aartsen et al. (2015)). The arrival times and directions of events within the dataset are fed to a likelihood function which is then used to perform a likelihood ratio test to compare a signal plus background hypothesis for the data to the background only hypothesis.

Construction of this likelihood function begins with the assignment of individual event probabilities that reflect the likelihood of seeing an event i with arrival time t_i,

reconstructed direction $\mathbf{x}_i$, and angular uncertainty σ_i given a hypothetical source located at $\mathbf{x}_s$ with strength n_s having a Gaussian time profile with mean time t_0 and width σ_w.

$$\mathcal{P}_i(\mathbf{x}_i, t_i, \sigma_i | \mathbf{x}_s, n_s, t_0, \sigma_w) = \frac{n_s}{n_{\rm tot}} \mathcal{S}_i + \left(1 - \frac{n_s}{n_{\rm tot}}\right) \mathcal{B}_i \tag{1}$$

The $\mathcal{S}_i$ and $\mathcal{B}_i$ terms listed in Eq. 1 are the signal and background probability density functions (p.d.f.) respectively. The p.d.f.s used in this search differ slightly from those in previously reported searches in that they use no reconstructed energy information. The signal p.d.f. is given by

$$\mathcal{S}_i(|\mathbf{x}_i - \mathbf{x}_s|, t_i, t_o, \sigma_w, \sigma_i) = S_i(|\mathbf{x}_i - \mathbf{x}_s|, \sigma_i) \cdot T_i(t_i, t_o, \sigma_w) \tag{2}$$

where

$$S_i(|\mathbf{x}_i - \mathbf{x}_s|, \sigma_i) = \frac{\kappa}{4\pi \sinh \kappa} \exp\left(\kappa \cos |\mathbf{x}_i - \mathbf{x_s}|\right) \tag{3}$$

and

$$T_i(t_i, t_o, \sigma_w) = \frac{1}{\sqrt{2\pi}\sigma_w} \exp\left(-\frac{(t_i - t_o)^2}{2\sigma_w^2}\right) \tag{4}$$

The spatial component of the signal p.d.f., S_i, is the Kent-Fisher distribution (Kent 1982), and it represents a slight deviation in the signal p.d.f. definition with respect to previous searches (see Aartsen et al. (2014b)). This function is analogous to a 2-dimensional Gaussian distribution, but it is normalized to the 2-sphere rather than an infinite plane. The concentration parameter κ is determined by the event angular uncertainty and is defined as $\kappa = \sigma_i^{-2}$. The temporal component of the signal p.d.f., T_i, is simply a Gaussian with mean emission time of t_o and a width of σ_w.

The background p.d.f., $\mathcal{B}_i$, is derived from the final level data set which is dominated by background. It has the following form

$$\mathcal{B}_i(\mathbf{x}_i, t_i) = P_{BkgDec}(\delta_i) \frac{P_{BkgAz}(\alpha_i)}{T} \tag{5}$$

where T is the total livetime of the search, $P_{BkgDec}(\delta_i)$ is a p.d.f. describing the event declination distribution, and $P_{BkgAz}(\alpha_i)$ is a p.d.f. describing the event distribution in detector azimuth. These p.d.f.s are generated directly from data and do not depend on any background simulation.

The likelihood function itself is simply the product sum of all individual event probabilities:

$$\mathcal{L}(\mathbf{x}_s, n_s, t_0, \sigma_w) = \prod \mathcal{P}_i(|\mathbf{x}_i - \mathbf{x}_s|, n_s, t_i, t_0, \sigma_w, \sigma_i) \tag{6}$$

The ratio between the likelihood function values under the background only hypothesis ($n_s = 0$) and the signal plus background hypothesis is maximized through variation of the source parameters n_s, σ_w, and t_0. The test statistic $\hat{\lambda}$ is then defined as the maximum value of the likelihood ratio:

$$\hat{\lambda} = -2 \log \left[\frac{\sqrt{2\pi}\hat{\sigma}_w}{T} \frac{\mathcal{L}(n_s = 0)}{\mathcal{L}(\mathbf{x}_s, \hat{n}_s, \hat{t}_o, \hat{\sigma}_w)} \right] \tag{7}$$

with $\mathcal{L}(n_s = 0)$ corresponding to the likelihood of the null hypothesis and $\mathcal{L}(\mathbf{x}_s, n_s, \hat{t}_o, \hat{\sigma}_w)$ the likelihood of the signal plus background hypothesis with the best-fit values of the source parameters. Because this is a search for sources of finite duration over a timescale of limited duration, the number of potential short duration flares within the data set exceeds that of flares of longer duration leading to an effective trials factor. This results in a bias towards flares of shorter duration. We counteract this effect through the introduction of a marginalization term $T/\sqrt{2\pi}\hat{\sigma_w}$ in test statistic formulation which serves to penalize flares of shorter duration. This term also ensures that the test statistic will asymptotically follow a χ^2 distribution with degrees of freedom corresponding to the number of fitted parameters for data consisting solely of background events. More details about this term and its justification can be found in Braun et al. (2010).

The χ^2 behavior of the test statistic enables the value of the maximized test statistic $\hat{\lambda}$ to be used to estimate the pre-trials p-value of the best-fit flare through the invocation

of Wilks's theorem (Wilks 1938). Because this search attempts to look many times over the whole Northern sky, the actual significance of a given flare will need to be adjusted to account for the effective number of trials accrued during the sky scan. We use the procedure detailed in Aartsen et al. (2015) that involves scrambling the event arrival times in the final dataset which also serves to scramble event right ascension. The search is performed on the randomized background data set and the p-value of the most significant flare in the search is recorded. Many iterations are performed to build a distribution of p-values which can then be compared to the p-value of the result from the real data. The fraction of background trials that result in a p-value of equal or greater significance than the observed p-value dictates the probability that the observed result is simply the consequence of a random background fluctuation. This probability is referred to as the post-trials p-value and it represents the true significance of the search result with proper trials factor correction.

In order to preserve generality, the presented search makes no use of information outside of the data set to designate source regions or time periods of interest. Instead, each point in the sky over a declination band ranging from -5° to 90° is examined. This is accomplished by discretizing the sky into separate bins and letting the location of these bins serve as the location of a hypothetical flaring source. Maximization of the likelihood is then performed to obtain a test statistic $\hat{\lambda}$ for each bin. The first iteration of this scan uses a relatively coarse 2° by 2° binning. Following completion of this first scan, a followup scan with finer 0.5° by 0.5° binning is performed over coarse bins featuring a pre-trials p-value more significant than a predefined threshold ($-\log_{10}(\text{p-value}) > 1.75$). The result is a map of pre-trials p-values which shows the estimated significance of the best-fit flare hypothesis at each bin. The best-fit flare from the bin featuring the most significant maximized test statistic after both scans is returned as the hottest spot in the search.

4. Results and Interpretations

Applying the described analysis method to the unscrambled dataset yields the skymap of the pre-trials p-values shown in Figure 3. The most significant flare is located at (RA, Dec.) = (268.75°, 54.25°) with a signal strength n_s of 13.53 signal events and a width σ_w of 5.89 days with the peak occurring on MJD 56107 (2012 June 29). The pre-trials p-value for this flare is estimated at 6.68×10^{-5}. The post-trials probability of seeing such a flare in a data set consisting of background only is 56% indicating that this flare is entirely consistent with the background hypothesis of the data. Given this null result, we can set an upper

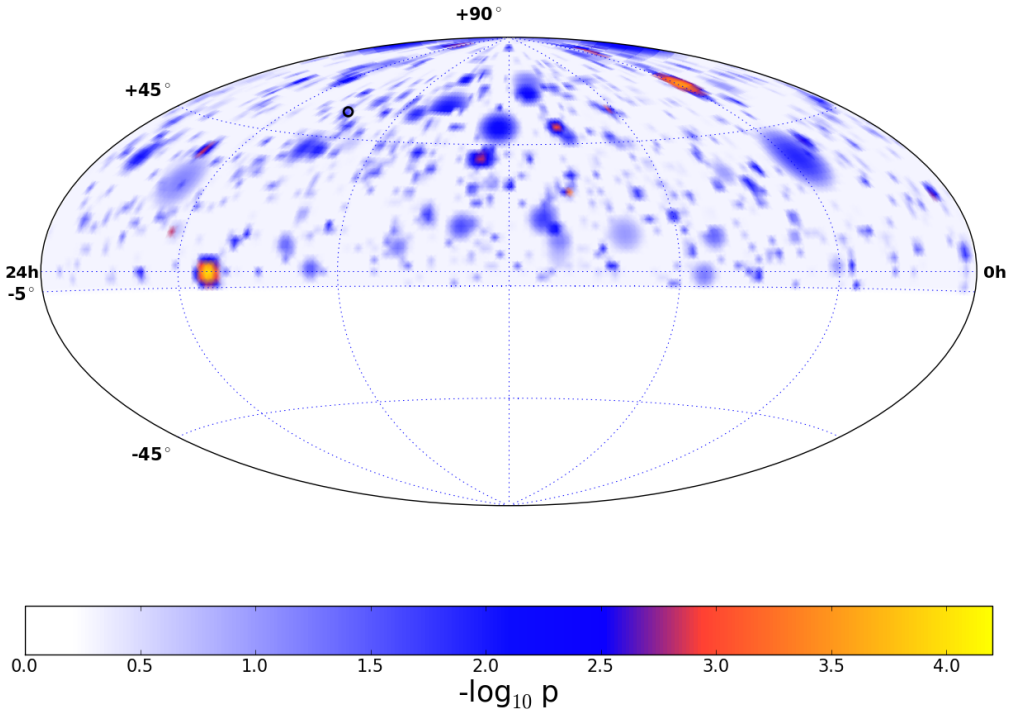

Fig. 3.— Sky map of pre-trials p-values for best fit flares per bin. The black circle identifies the location of the most significant flare found at RA = 268.75° and Declination = 54.25°.

limit on the neutrino flux of any possible unobserved neutrino flare that may have occurred during the search period.

4.1. Generic Source Limit

Due to the focus on low-energy events in this search, we choose to examine the limit with respect to a soft-spectrum E^{-3} generic flaring neutrino source with a Gaussian emission profile. An an upper limit is established through signal injections at a specified location. First, the background p-value distribution at the chosen location is constructed from several time scramblings of the data. Signal events are then injected with some Poisson mean value that is increased until the recovered p-values from the injections exceed the median background p-value 90% of the time. This Poisson mean number of signal events is then taken as an event upper limit for the analysis method.

The upper limit on a generic flaring source for several emission timescales and choices of declination is plotted in Figure 4. The limit rises at longer timescales as the rate of accidental background correlations becomes non-negligible. A limit on the time-integrated flux ($\mathrm{GeV}^{-1}\cdot\ \mathrm{cm}^{-2}$) is plotted as well. This limit is obtained by folding the source spectrum with the effective area of the event selection and normalizing the flux so that the number of events produced in the detector corresponds to the calculated Poisson mean event upper limit.

4.2. Choked GRB Limits

This null result can also be used to construct limits on specific neutrino emission models such as the model for choked GRB emission by Razzaque et al. (2004) and Ando & Beacom (2005) mentioned previously (this will hereafter be referred to as RMW/AB).

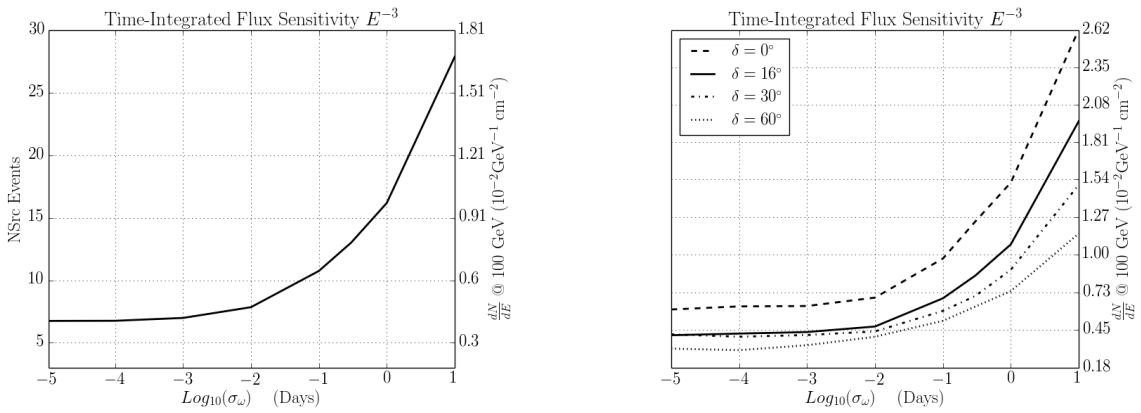

Fig. 4.— Upper limit (90% C.L.) for a generic E^{-3} transient source as a function of flare width σ_w.The limit is given in mean number of events (left axis) as well as in time-integrated flux at a reference energy of 100 GeV (right axis).

Unlike the hard spectra sources (e.g, E^{-2}) that are the typical target in IceCube searches, the neutrino flux for choked GRBs is predicted to be much softer. The spectral shape can be modeled via a doubly broken power law with spectral breaks occurring as hadronic ($E_{\nu^{(1)}}$) and radiative ($E_{\nu^{(2)}}$) cooling mechanisms become efficient respectively (see Eq. 8).

$$\frac{d\Phi_\nu}{dE} = F_\nu \begin{cases} E^{-2} & E > E_\nu^{(1)} \\ E_\nu^{(1)} E^{-3} & E_\nu^{(1)} < E < E_\nu^{(2)} \\ E_\nu^{(1)} E_\nu^{(2)} E^{-4} & E_\nu^{(2)} < E < E_{max} \end{cases} \tag{8}$$

$$F_\nu = \frac{< n >_{\pi(K)} B_{\pi(K)}}{8} \cdot \frac{E_j \Gamma_b^2}{2\pi D^2 \ln(E'_{p,max}/E'_{p,min})} \tag{9}$$

The fluence F_ν at Earth is given by Eq. 9 and depends upon the pion (kaon) multiplicity $< n >$, neutrino production branching ratio for pions (kaons) $B_{\pi(K)}$, minimum and maximum proton energies ($E'_{p,min}, E'_{p,max}$), kinetic energy of the jet E_j, bulk Lorentz factor Γ_b, and lastly the distance to the source D. Equations 8 and 9 reveal that the normalization and spectral shape of the neutrino flux at Earth are highly dependent on the kinetic energy of the jet E_j and the bulk lorentz factor Γ_b. We therefore choose to examine the predicted

neutrino fluence in E_j-Γ_b phase space.

To ascertain which values of these parameters produce a fluence detectable through our search method, an event upper limit is first determined via the injection of signal events following a spectrum set by the value of E_j and Γ_b (the same process used to generate an event upper limit for the generic E^{-3} scenario). This event upper limit then is then combined with the effective area of the event selection to determine the neutrino fluence necessary for detection. For a given choice of E_j and Γ_b this sets a limit on the distance at which the source would still be visible to the search; we define this distance D_{vis} as the visibility distance.

When combined with the area of sky examined by the search Ω_A, this visibility distance in turn defines a parameter dependent volume V_A over which the search method monitors where $V_A = \frac{1}{3}\Omega_A D_{vis}^3$. The monitored volume V_A corresponds to the volume in which a choked GRB event would have been detected by the search method with 90% confidence (assuming jet alignment). If the observation period of the search is considered, this monitored volume can be converted into a limit on the volumetric rate of choked GRB events as a function of E_j and Γ_b. This requires two assumptions to be made however: 1) The jets of any choked GRB event in this volume are aligned with Earth and 2) The nearby universe is homogeneous with respect to CC SNe production. The rate limit is then given by

$$R = \left(\frac{U.L.(0|\mu)}{\tau \cdot V_A} \right) \tag{10}$$

where τ is the livetime of the search, V_A is the monitored volume previously defined, and $U.L.(0|\mu)$ is the null observation upper limit on the number of choked GRBs that occurred in our monitored volume with background expectation of μ. Many iterations of the search performed with only background data determined the probability of a background false positive rate to be very small ($\leq 10^{-3}$). We therefore take $\mu \approx 0$ leading to a Neyman

upper limit of 2.3 from the null observation.

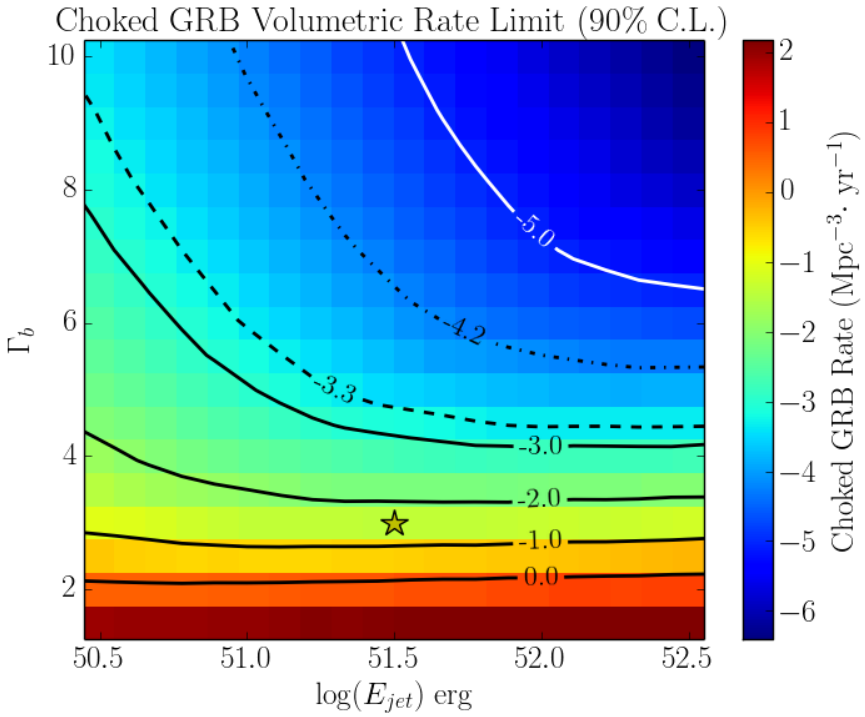

Fig. 5.— Histogram of the rate limit on choked GRBs in the nearby universe. The bin for canonical values of the RMW/AB emission model is marked by the star. The dashed line contour gives the rate of core-collapse supernovae within 10 Mpc as measured by Kistler et al. (2011). The dot-dashed line is the volumetric rate extracted from a large survey of SNe in the local universe (Leaman et al. 2011)

The volumetric rate limit for a range of values of jet kinetic energy and bulk Lorentz factor is plotted in Figure 5. In addition to the calculated volumetric rate limits, two separate measurements of the nearby CC SNe are also plotted to provide context to the limits. Choked GRB events harboring particularly energetic jet parameters should be visible to the search method. If one compares the limits for the canonical model parameter values ($\Gamma_b = 3$, $E_j = 10^{51.5}$ erg) to the CC SNe rates, it is clear that the search method is

not very sensitive to large regions of the model parameter space in its current state. The capabilities of future iterations of this type of search should be considerably improved as both the event selection and analysis methods are refined.

5. Conclusions

The described search examined a newly developed data set consisting of 30-300 GeV muon neutrinos. No evidence for transient astrophysical neutrino sources was found in the data, leading to the construction of upper limits on the neutrino fluence of potential sources within the observation period. In particular, we examine the derived limit in the context of neutrino emission from choked GRBs. Although this search in its current configuration is only sensitive to particularly energetic or nearby choked GRBs, the sensitivity of this method will improve as the event selection and search techniques are further optimized for muon neutrino events at sub-TeV energies. Most importantly, continued development of this event selection will complement the current mature IceCube analyses at higher energies, leading to an overall enhancement of the detector's sensitivity to transient sources.

We acknowledge support from the following agencies: U.S. National Science Foundation-Office of Polar Programs, U.S. National Science Foundation-Physics Division, University of Wisconsin Alumni Research Foundation, the Grid Laboratory Of Wisconsin (GLOW) grid infrastructure at the University of Wisconsin - Madison, the Open Science Grid (OSG) grid infrastructure; U.S. Department of Energy, and National Energy Research Scientific Computing Center, the Louisiana Optical Network Initiative (LONI) grid computing resources; Natural Sciences and Engineering Research Council of Canada, WestGrid and Compute/Calcul Canada; Swedish Research Council, Swedish Polar Research Secretariat, Swedish National Infrastructure for Comput ing (SNIC), and Knut and Alice

Wallenberg Foundation, Sweden; German Ministry for Education and Research (BMBF), Deutsche Forschungsgemeinschaft (DFG), Helmholtz Alliance for Astroparticle Physics (HAP), Research Department of Plasmas with Complex Interactions (Bochum), Germany; Fund for Scientific Research (FNRS-FWO), FWO Odysseus programme, Flanders Institute to encourage scientific and technological research in industry (IWT), Belgian Federal Science Policy Office (Belspo); University of Oxford, United Kingdom; Marsden Fund, New Zealand; Australian Research Council; Japan Society for Promotion of Science (JSPS); the Swiss National Science Foundation (SNSF), Switzerland; National Research Foundation of Korea (NRF); Danish National Research Foundation, Denmark (DNRF).

REFERENCES

Aartsen, M. G., Abbasi, R., Abdou, Y., et al. 2014a, Nuclear Instruments and Methods in Physics Research A, 736, 143

Aartsen, M. G., Ackermann, M., Adams, J., et al. 2014b, ApJ, 796, 109

Aartsen, M. G., Ackermann, M., Adams, J., et al. 2015, The Astrophysical Journal, 807, 46

Abbasi, R., Abdou, Y., Abu-Zayyad, T., et al. 2012, Astroparticle Physics, 35, 615

Adrián-Martínez, S., Samarai, I. A., Albert, A., et al. 2012, ApJ, 760, 53

Ahrens, J., Bai, X., Bay, R., et al. 2004, Nuclear Instruments and Methods in Physics Research A, 524, 169

Ando, S., & Beacom, J. F. 2005, Physical Review Letters, 95, 061103

Becker, J. K., & Biermann, P. L. 2009, Astroparticle Physics, 31, 138

Braun, J., Baker, M., Dumm, J., et al. 2010, Astroparticle Physics, 33, 175

Braun, J., Dumm, J., De Palma, F., et al. 2008, Astroparticle Physics, 29, 299

IceCube Collaboration, Achterberg, A., Ackermann, M., et al. 2006, Astroparticle Physics, 26, 155

Kent, J. T. 1982, Journal of the Royal Statistical Society. Series B (Methodological), 44, pp. 71

Kistler, M. D., Yüksel, H., Ando, S., Beacom, J. F., & Suzuki, Y. 2011, Phys. Rev. D, 83, 123008

Leaman, J., Li, W., Chornock, R., & Filippenko, A. V. 2011, Monthly Notices of the Royal Astronomical Society, 412, 1419

473 Modjaz, M. 2011, Astronomische Nachrichten, 332, 434

474 Murase, K., Kashiyama, K., & Mészáros, P. 2013, Physical Review Letters, 111, 131102

475 Neunhöffer, T. 2006, Astroparticle Physics, 25, 220

476 Razzaque, S., Mészáros, P., & Waxman, E. 2004, Physical Review Letters, 93, 181101

477 Rees, M. J., & Meszaros, P. 1992, Monthly Notices of the Royal Astronomical Society, 258,
478 41P

479 Taboada, I. 2010, Phys. Rev. D, 81, 083011

480 Thrane, E., Abe, K., Hayato, Y., et al. 2009, ApJ, 704, 503

481 Whitehorn, N., van Santen, J., & Lafebre, S. 2013, Computer Physics Communications,
482 184, 2214

483 Wilks, S. S. 1938, Ann. Math. Statist., 9, 60

484 Woosley, S. E., & Bloom, J. S. 2006, Annual Review of Astronomy & Astrophysics, 44, 507